



RESEARCH LETTER

10.1002/2015GL064955

Key Points:

- Unambiguous evidence of deep injections of MeV electrons from multispacecraft
- Extremely large electric fields (50 mV/m) associated with the dipolarization
- Strong dipolarizations may supply significant MeV electrons to radiation belts

Correspondence to:

L. Dai,
ldai@spaceweather.ac.cn

Citation:

Dai, L., et al. (2015), Near-Earth injection of MeV electrons associated with intense dipolarization electric fields: Van Allen Probes observations, *Geophys. Res. Lett.*, *42*, 6170–6179, doi:10.1002/2015GL064955.

Received 15 JUN 2015

Accepted 16 JUL 2015

Accepted article online 20 JUL 2015

Published online 10 AUG 2015

Near-Earth injection of MeV electrons associated with intense dipolarization electric fields: Van Allen Probes observations

Lei Dai^{1,2}, Chi Wang¹, Suping Duan¹, Zhaohai He¹, John R. Wygant², Cynthia A. Cattell², Xin Tao³, Zhenpeng Su³, Craig Kletzing⁴, Daniel N. Baker⁵, Xinlin Li⁵, David Malaspina⁵, J. Bernard Blake⁶, Joseph Fennell⁶, Seth Claudepierre⁶, Drew L. Turner⁶, Geoffrey D. Reeves⁷, Herbert O. Funsten⁷, Harlan E. Spence⁸, Vassilis Angelopoulos⁹, Dennis Fruehauff¹⁰, Lunjin Chen¹¹, Scott Thaller², Aaron Breneman², and Xiangwei Tang²

¹State Key Laboratory of Space Weather, National Space Science Center, Chinese Academy of Sciences, Beijing, China, ²School of Physics and Astronomy, University of Minnesota, Twin Cities, Minneapolis, Minnesota, USA, ³Department of Geophysics and Planetary Sciences, University of Science and Technology of China, Hefei, China, ⁴Department of Physics and Astronomy, University of Iowa, Iowa City, Iowa, USA, ⁵Laboratory for Atmospheric and Space Physics, University of Colorado Boulder, Boulder, Colorado, USA, ⁶Space Sciences Department, The Aerospace Corporation, Los Angeles, California, USA, ⁷Los Alamos National Laboratory, Los Alamos, New Mexico, USA, ⁸Department of Physics Institute for Earth, Oceans and Space, University of New Hampshire, Durham, New Hampshire, USA, ⁹Department of Earth, Planetary and Space Sciences and Institute of Geophysics and Planetary Physics, University of California, Los Angeles, California, USA, ¹⁰Institute of Geophysics and extraterrestrial Physics, Braunschweig University of Technology, Braunschweig, Germany, ¹¹Department of Physics, University Of Texas at Dallas, Richardson, Texas, USA

Abstract Substorms generally inject tens to hundreds of keV electrons, but intense substorm electric fields have been shown to inject MeV electrons as well. An intriguing question is whether such MeV electron injections can populate the outer radiation belt. Here we present observations of a substorm injection of MeV electrons into the inner magnetosphere. In the premidnight sector at $L \sim 5.5$, Van Allen Probes (Radiation Belt Storm Probes)-A observed a large dipolarization electric field (50 mV/m) over ~ 40 s and a dispersionless injection of electrons up to ~ 3 MeV. Pitch angle observations indicated betatron acceleration of MeV electrons at the dipolarization front. Corresponding signals of MeV electron injection were observed at LANL-GEO, THEMIS-D, and GOES at geosynchronous altitude. Through a series of dipolarizations, the injections increased the MeV electron phase space density by 1 order of magnitude in less than 3 h in the outer radiation belt ($L > 4.8$). Our observations provide evidence that deep injections can supply significant MeV electrons.

1. Introduction

Substorm dipolarization is known to inject energetic electrons into the radiation belts. Injected electrons are usually in the energy range from tens of keV to hundreds of keV. Observations and model results from the last two decades, however, indicate that dipolarizations sometimes inject MeV electrons, as well. In test particle simulations, Kim *et al.* [2000] showed that dipolarizations can contribute to MeV electrons enhancements in the outer radiation belt. Ingraham *et al.* [2001] provided observational evidence that strong substorms continuously inject MeV electrons to the geosynchronous altitude. Using data from the Akebono spacecraft, Nagai *et al.* [2006] identified rapid enhancements of MeV electrons associated with storm time substorm dipolarizations in the outer radiation belt. Modeling results from Fok *et al.* [2001] and Glocer *et al.* [2011] attributed rapid enhancements of MeV electrons in their modeling results to dipolarization electric fields. Using data from multiple spacecraft that tracked the electron phase space density (PSD) at different radial locations, Dai *et al.* [2014] showed that strong dipolarization electric fields injected MeV electrons by pushing magnetotail electrons to the geosynchronous altitude. Su *et al.* [2014] provided evidence from the Van Allen Probes (Radiation Belt Storm Probes (RBSP)) measurements that substorm injections of MeV electrons, as well as acceleration by chorus waves, contribute to the outward extension of the outer belt.

Substorm injections of MeV electrons are interesting from several perspectives. Their contribution to the energization of MeV electron in the radiation belt is relatively underexplored. The efficiency of this

©2015. The Authors.

This is an open access article under the terms of the Creative Commons Attribution-NonCommercial-NoDerivs License, which permits use and distribution in any medium, provided the original work is properly cited, the use is non-commercial and no modifications or adaptations are made.

energization under different solar wind conditions and various levels of geomagnetic activity is unclear. Much of the physics of MeV electron injection remains to be explored. It now appears that only a small portion of substorm dipolarizations can inject MeV electrons. The special conditions under which substorm dipolarizations can inject MeV electrons are unknown. Furthermore, injections have been considered to provide the seed population needed for the local energization through wave-particle interactions. Injections of MeV electrons provide a harder spectrum of seed populations than injections of tens to hundreds of keV electrons.

The electric field associated with dipolarizations, in which magnetic field lines collapse from a tail-like shape to a more dipole-like shape [Baker *et al.*, 1996], is believed to drive particle acceleration and injections [Birn *et al.*, 2013]. In observations, dipolarization electric fields are time varying, are azimuthally localized, and can be from mV/m to tens of mV/m [e.g., Cattell and Mozer, 1984; Fairfield *et al.*, 1998; Tu *et al.*, 2000; Dai *et al.*, 2014]. Inspired by the injection front model [Moore *et al.*, 1981], Li *et al.* [1998] constructed a model of an earthward propagating electric field pulse to simulate the substorm injection. In the model of Li *et al.* [1998], the electric field pulse is associated with a rapid increase in B_z to represent the dipolarization. The model can produce signals of injections at different radial distances [Li *et al.*, 1998; Sarris *et al.*, 2002; Li *et al.*, 2003; Zaharia *et al.*, 2004; Liu *et al.*, 2009]. Gabrielse *et al.* [2012] developed a similar model, adding the ingredient of twin vortices and their dawnward electric fields that are adjacent to the edge of the earthward flow. Alternative approaches to model the electric field and plasma dynamics of substorm dipolarizations involve MHD simulations [Birn *et al.*, 1998; Fok *et al.*, 2006; Birn *et al.*, 2013; Ashour-Abdalla *et al.*, 2011] and Rice Convection Model(RCM)-based simulations [Zhang *et al.*, 2009; Yang *et al.*, 2011].

Injected particles are trapped on closed orbits as the dipolarization electric field is reduced or diminished. As a result, deep injections can directly supply energetic particles to the center of the outer radiation belt. Using the CRRES data set, Friedel *et al.* [1996] showed that injections can penetrate to $L = 4$. Such near-Earth injection events are also manifested as penetrating electric fields [Rowland, 2002]. Sergeev *et al.* [1998] documented short-duration injections that correlate with dawn-dusk electric fields at a radial distance of $\sim 5R_E$. In a study of multiple events, Reeves *et al.* [1996] showed that the injection region traveled earthward at an average of 24 km/s from the geosynchronous altitude to the CRRES satellite. Turner *et al.* [2015] provided evidence of substorm-associated injections observed down to $L = 2.5$.

The orbit of Van Allen Probes (RBSP) [Mauk *et al.*, 2012] is suitable for studying near-Earth injections. To better understand MeV electron injections in the RBSP data set, we need to investigate the spatial scales of the injection region, the properties of the electric fields and magnetic fields, the characteristics of MeV electrons, and how many MeV electrons are injected during the dipolarizations. In this paper, we present detailed field and particle observations from RBSP, Time History of Events and Macroscale Interactions during Substorms (THEMIS), Los Alamos National Laboratory (LANL)-GEO, and GOES of a MeV electron injection event in the inner magnetosphere. Previous observations of MeV electron injections has one limitation—only dispersionless injections were observed. In this study, we provide an unambiguous injection signature of the dispersed and drifting electron population up to ~ 3 MeV. This event is notable because of an extremely large dipolarization electric field 50 mV/m that is rarely seen in previous models and observations.

2. Observations of Near-Earth Injection of MeV Electrons

2.1. Overview of RBSP-A Observations on 26 April 2013

With its apogee near midnight, RBSP-A spent several hours at $L = 5 - 6$ in the nightside on 26 April 2013. RBSP-B is not in an ideal orbit location to be relevant for this study. Figure 1 shows solar wind conditions, geomagnetic conditions, and an overview of fields and energetic particles from RBSP-A from 03 UT to 09 UT on 26 April 2013. As shown in Figure 1a, the solar wind dynamic pressure was steady. The $SYM-H$ index from -20 to -50 covered part of the main phase and the recovery phase in a moderate storm (see Figure 1b). The AE index increased from 400 to ~ 1000 at around 0510 UT. The substorm around 0510 UT is selected for analysis. Intuitively, intense solar wind and large geomagnetic storms may have more free energy to drive MeV electron injection events. However, this event and similar events in previous studies indicate frequent occurrence of MeV electron injections during moderate activity, suggesting a complex chain of processes through which MeV electron injections can drain free energy from the magnetosphere.

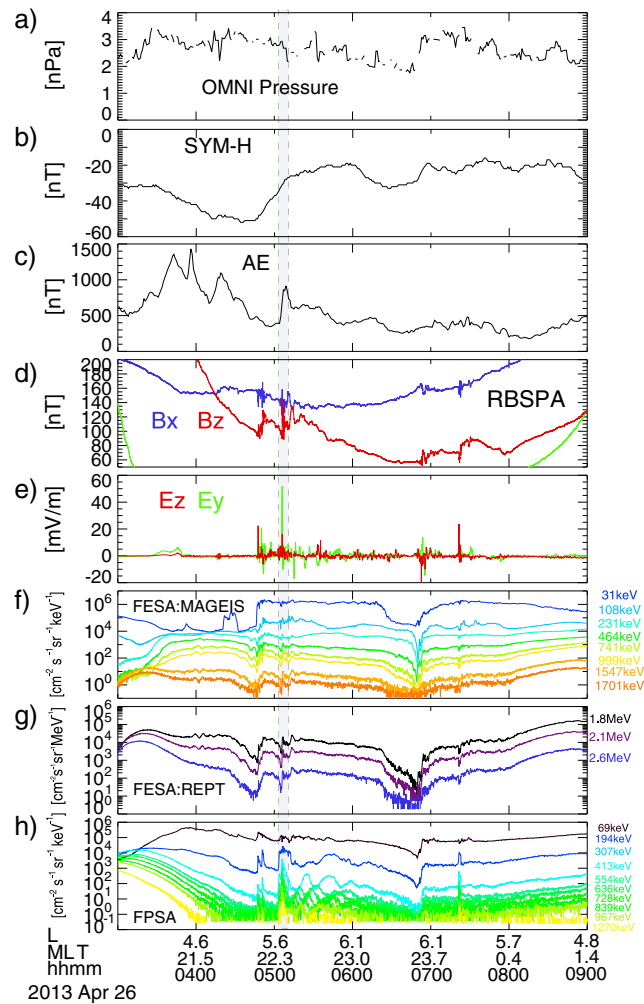


Figure 1. Overview of solar wind conditions, the geomagnetic activity and RBSP-A observations on 26 April 2013. (a) One minute OMNI data of the solar wind dynamic pressure. (b) The SYM-H index. (c) AE index. (d) One second resolution B_x and B_z components in GSM from RBSP-A. (e) Spin fit E_y and E_z in MGSE from RBSP-A. (f) The different flux of energetic electrons from MagEIS onboard RBSP-A. (g) The different flux of energetic electrons from REPT onboard RBSP-A. (h) The different flux of energetic ions from MagEIS onboard RBSP-A.

Figures 1d and 1e show the DC magnetic field and electric field from RBSP-A. The magnetic field data are the 1 s resolution data from the Electric and Magnetic Field Instrument Suite and Integrated Science (EMFISIS) fluxgate magnetometer [Kletzing et al., 2013]. The typical dipolarization signal is a rapid increase in B_z that is often associated with a decrease in B_x . In Figure 1d, several dipolarizations with different time scales can be clearly identified from about 0440 UT to 0740 UT. The spin resolution electric field from the Electric Field and Waves (EFW) instrument [Wygant et al., 2013] in the modified GSE coordinates is shown in Figure 1e. E_z and E_y are in the spin plane and close to the GSE z and GSE y within 20° . In the regime of DC and ULF wave measurement, the electric field component E_x along the spin axis can be deduced from the $\mathbf{E} \cdot \mathbf{B} = 0$ assumption if the angle between \mathbf{B} , and the spin plane is larger than 15° [Dai et al., 2013]. Electric field pulses of more than 20 mV/m were frequently seen during dipolarizations on this day. In particular, the duskward electric field was as large as 50 mV/m during the dipolarization around 0505 UT.

2.2. Dipolarization Front and the Dispersionless Injection at RBSP

Figures 2a–2h present an expanded view of the substorm injection at RBSP-A from 0445 UT to 0515 UT. An abrupt increase from 100 nT to 140 nT in the northward magnetic component B_z , usually referred to as a dipolarization front (DF) [Nakamura et al., 2002; Runov et al., 2009; Ge et al., 2011; Fu et al., 2011; Hwang et al., 2011; Zhou et al., 2014], is identified around 0506 UT in Figure 2b and marked by the gray bar. The DF, which lasted about 40 s from 05:05:40 UT to 05:06:20 UT, was accompanied by an extremely large dawn-dusk electric field E_y and a rapid increase in 30 keV to 2.6 MeV electrons. The dawn-dusk dipolarization electric field corresponded to a large earthward $\mathbf{E} \times \mathbf{B}$ in panel Figure 2d. Even though it decelerates in the near-Earth region, a high-speed bursty bulk flow [Angelopoulos et al., 1992] may occasionally penetrate deep into the inner magnetosphere. Because of the large B_x in the inner magnetosphere, the DF was also related to a large

Figures 1f, 1g, and 1h show the electron and ion flux from the RBSP Energetic Particle, Composition, and Thermal Plasma (ECT) [Spence et al., 2013]. Figure 1f shows the electron differential flux from Magnetic Electron Ion Spectrometer (MagEIS) [Blake et al., 2013] in the 31 keV to 1.7 MeV energy range. Electron of 10–100 keV can increase by 2 orders of magnitude during dipolarizations. Figure 1g shows the electron differential flux in the first three energy channels (1.8 MeV, 2.1 MeV, and 2.6 MeV) from Relativistic Electron-Proton Telescope (REPT) [Baker et al., 2013]. Figure 1h shows the differential flux of energetic ions from 69 keV to 1.2 MeV from MagEIS. In the substorm dipolarization near 0505 UT, injected MeV ions were followed up by drift echos signals.

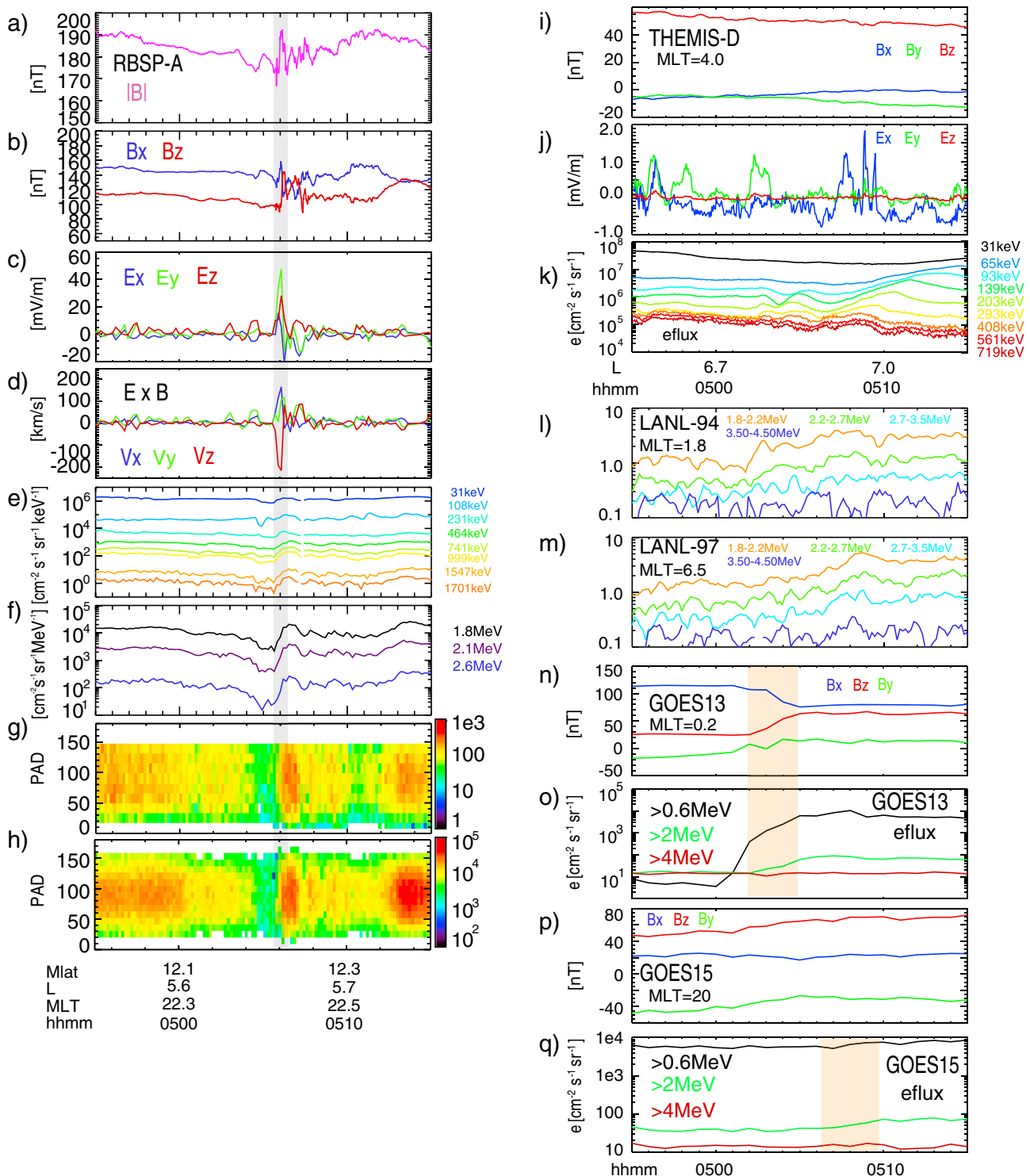


Figure 2. The 20 min expanded view of the injection event from 0445 UT to 0515 UT. RBSP-A measurements of (a) the magnitude of \mathbf{B} , (b) B_x and B_z in GSM, (c) the spin fit electric field in GSM (the spin axis electric field is obtained from the $\mathbf{E} \times \mathbf{B} = 0$ assumption), (d) the $\mathbf{E} \times \mathbf{B}$ drift velocity in GSM, (e) fluxes of energetic electrons from MagEIS, (f) fluxes of energetic electrons from REPT, (g) PAD of 0.9 MeV electrons from MagEIS, (h) PAD of 1.8 MeV electrons from REPT. THEMIS-D measurements of (i) the spin resolution magnetic field in GSM, (j) the spin resolution electric field in GSM, (k) differential energy fluxes of energetic electrons from SST. (l and m) Counts per second of MeV electrons (averaged over 20 s) measured from LANL 94 and LANL 94, respectively. (n and o) GOES 13 measurements of three magnetic field components in GSM and the integral flux of energetic electrons. (p and q) are GOES 15 measurements of three magnetic field components in GSM and the integral flux of energetic electrons.

V_z ($\sim -E_y/B_x$) toward the equatorial plane. In addition, E_z corresponded to a flow deflected toward flanks at about 100 km/s, likely due to the rising pressure in the inner magnetosphere.

The electron injection of electrons at RBSP-A was dispersionless (Figures 2e and 2f). As shown in Figures 2g and 2h, the pitch angle distribution (PAD) of injected MeV electrons was more concentrated around 90° at the DF and thereafter spread out in a more isotropic distribution. The major acceleration mechanisms of electrons in dipolarizations, betatron acceleration and Fermi acceleration, are characterized by an energy increase associated with the perpendicular and parallel velocities, respectively [Northrop, 1963; Birn *et al.*, 2013; Fu *et al.*, 2011]. The PAD observations thus indicate that the acceleration of MeV electrons at the DF is mostly caused by betatron acceleration. Before the DF, energetic electrons appear to drop out due to the stretching of field lines. Behind the dipolarization front from 05:06:10 UT to 05:07:10 UT was the high B_z region, usually referred to as the dipolarizing flux bundle (DFB) [Liu *et al.*, 2013]. The DFB was associated with an elevated flux of energetic electrons.

2.3. The Dispersive Injection at THEMIS-D

Figures 2i–2k present the simultaneous observations from THEMIS-D from 0445 UT to 0515 UT in the predawn sector (MLT = 4) at $L \sim 7$. Because of the dipolarization's azimuthal localization, THEMIS-D did not observe the dipolarization signals. After 0506 UT, THEMIS-D observed an increase in 720 keV electron fluxes followed by increases in lower energy electron fluxes, usually referred to as a dispersed injection. Such dispersion signals result from the energy dependence of electron drift velocities after electrons are released simultaneously from an injection region [e.g., Reeves *et al.*, 1991]. From the timing difference of the initial flux increases, the injected electrons at THEMIS-D corresponded to a release of dispersionless electrons at \sim MLT = 2–3 around 0505–0506 UT.

2.4. Signals of MeV Electron Injection From LANL-GEO and GOES at Geosynchronous Altitude

The LANL 94 and LANL 97 spacecraft were at MLT \sim 1.8 and \sim 6.5, respectively. Figures 2l and 2m show MeV electron observations from these two spacecraft. LANL 94 was near the eastern edge of the injection region, and LANL 97 was outside the injection region. Starting from 0502 UT, LANL 94 observed an injection of MeV electrons. The onset time was close to that at GOES 13 shown in Figure 2o. Dispersed, drifting electron populations up to 3 MeV, an unambiguous signature of MeV electron injections, were clearly seen by LANL 97 from 0506 UT.

The GOES 13 and GOES 15 spacecraft were on the nightside, monitoring the injection at the geosynchronous altitude. Figures 2n–2q show GOES 13 and GOES 15 observations of the magnetic fields and energetic particles. Starting from \sim 0502 UT, GOES 13, which was at the midnight within the injection region, observed a sustained dipolarization associated with injection of >0.6 MeV and >2.0 MeV electrons. The dipolarization at GOES 13 involved an increase of B_z toward an elevated level. This type of dipolarization is usually thought of as a global dipolarization that is possibly related to but distinct from a dipolarization front [Nakamura *et al.*, 2011].

Based on the 2–3 min timing difference of the maximum electron flux increases at GOES 13 and RBSP-A, we obtain a 40–60 km/s earthward propagation velocity of the injection region from GOES 13 to RBSP-A. This slow earthward propagation of the injection region is consistent with those in previous statistical studies by Moore *et al.* [1981] and Reeves *et al.* [1996]. Similar to THEMIS-D, GOES 15 was located outside the injection region. Dipolarization signals were absent at GOES 15. From 0507 UT to 0508 UT, the injection started to populate the electrons at the geosynchronous altitude. As a result, GOES 15 observed a persistent increase in >0.6 MeV and >2.0 MeV electron fluxes.

2.5. Increases of MeV Electron PSD in the Outer Radiation Belt

Several injections occurred between 05 UT and 08 UT on 26 April. Figure 3 presents the electron PSD as a function of the first and second adiabatic invariant from RBSP-A in 5 h before and after the injections. The electron PSD is plotted at the fixed second adiabatic invariant $K = 0.1 \pm 0.02$ G^{1/2} km and first adiabatic invariant $\mu = 1000 \pm 20, 1500 \pm 20, 2000 \pm 20$ MeV/G. The PSD is presented in the Geospace Environment Modeling units (c/MeV/cm)³ [Chen *et al.*, 2005]. The parameter K is evaluated based on the T04 models [Tsyganenko and Sitnov, 2005] and available from the Ephemeris data files on the RBSP ECT website. Note that there is uncertainty (10–20%) in K due to the inaccuracy of the magnetic field model near the injection region. This magnitude of uncertainty in K is expected to produce very little difference in Figure 3. The selected set of μ and K approximately corresponds to 1–2 MeV electrons mirrored at low magnetic latitude at the

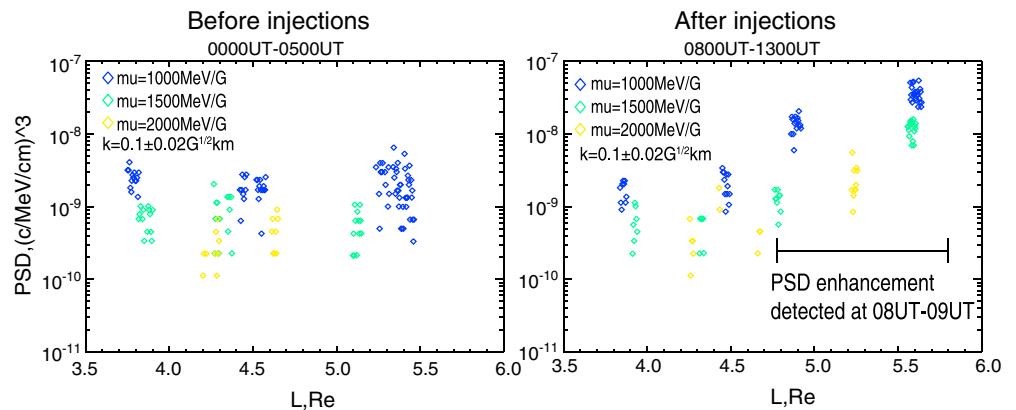


Figure 3. The electron PSD at fixed K and μ (left) before the injections and (right) after the injections.

geosynchronous altitude. Before the injections, the PSD at $\mu = 1000 \text{ MeV/G}$ is $10^{-9} - 10^{-8} (\text{c/MeV/cm})^3$ at $L = 4 - 5.5$. After the injections, the electron PSD at $\mu = 1000 \text{ MeV/G}$ increased by an order of magnitude from 10^{-9} to $10^{-8} (\text{c/MeV/cm})^3$ at $L = 4.8 - 5.6$. The PSD of higher energy electrons at $\mu = 1500 \text{ MeV/G}$ and $\mu = 2000 \text{ MeV/G}$ increased by 1 order of magnitude as well. The increases of MeV electrons at $L = 4.8 - 5.7$ were detected between 08 UT and 09 UT, indicating that the acceleration of MeV electrons was finished before 08 UT, fewer than 3 h after the injection. The 3 h time scale is generally less than that characterized by whistler wave-driven acceleration ($\sim 10 \text{ h}$) or radial diffusion ($\sim 1 \text{ day}$).

In the following, we examine if whistler wave-driven acceleration or radial diffusion can be responsible for the enhancement in Figure 3. We first estimate the wave power needed to produce the observed fast acceleration ($\sim 3 \text{ h}$) by local wave acceleration. The time scale for the energization can be estimated as $1/(D_{EE}/E^2)$, where D_{EE} is the diffusion coefficient in the energy space and E is the energy of particles. D_{EE} is proportional to the wave power B_w^2 of the whistler waves. According to a previous whistler wave model by [Horne *et al.*, 2005], it took $\sim 20 \text{ h}$ for whistler waves with amplitude 50–100 pT to increase the flux of 1 MeV electrons by 1 order of magnitude. In our event, the acceleration occurs within less than 3 h. For wave acceleration to be viable in this event, we need a continuous presence of strong whistler waves with amplitude $> 200 \text{ pT}$. Assume a few hundred Hz bandwidth of the whistler waves, the required wave power is larger than $10^{-4} \text{ nT}^2/\text{Hz}$. Figure 4 shows the observed wave power B_w^2 from RBSP-A and THEMIS-E. At the nightside, RBSP-A did not see the required strong whistler wave activity. Lower band ($< 0.5f_{ce}$) whistler waves are sparsely observed from 0520 UT to 0600 UT and from 0730 UT to 0840 UT. The power of whistler waves was mostly less than $10^{-6} \text{ nT}^2/\text{Hz}$, more than 2 orders of magnitude less than that of the whistler waves considered to effectively energize MeV electrons [Su *et al.*, 2014]. At the dawnside, THEMIS-D was at large L ($L = 6.7 - 9.8$) from 05 UT to 08 UT; THEMIS-E encountered $L = 4 - 5.7$ at dawn around 0630 UT–0710 UT and did not observe strong whistler waves (Figure 4d). According to the statistical result Li *et al.* [2009], strong ($> 100 \text{ pT}$) whistler waves have a higher occurrence rate at nightside and dawnside. With an absence of continuous strong whistler waves at nightside (RBSP-A) and dawnside (THEMIS-E) in this event, it is highly unlikely to have strong whistler waves at other locations during this 3 h time period. Thus, we conclude that whistler wave-driven acceleration is unlikely to produce the electron enhancement in Figure 3.

Now we estimate whether radial diffusion is possible to produce the acceleration. How quickly radial diffusion can occur is proportional to the power of random wave fields in the ULF frequency band. ULF waves can be driven by solar wind or sources internal to the magnetosphere. Figures 4c and 4e show the ULF power spectra from RBSP and THEMIS for this event. At RBSP-A, most Fourier power from 05 UT to 08 UT is due to the zigzag shape of \mathbf{B} in dipolarizations. A zigzag shape naturally corresponds to a broadband Fourier power spectrum. But these broadband power spectra are not random fluctuations which can lead to radial diffusion. Only around 06 UT and 08 UT there were some ULF wave spectra ($10^2 - 10^3 \text{ nT}^2/\text{Hz}$) that may cause radial diffusion. The ULF wave power observed by THEMIS-E is $10^1 - 10^2 \text{ nT}^2/\text{Hz}$, 1 order magnitude smaller. The observed ULF wave spectra, which are comparable to or less than those in past statistic results [Ozeke *et al.*, 2012], are too weak and sporadic to cause fast radial diffusion in less than 3 h in this event.

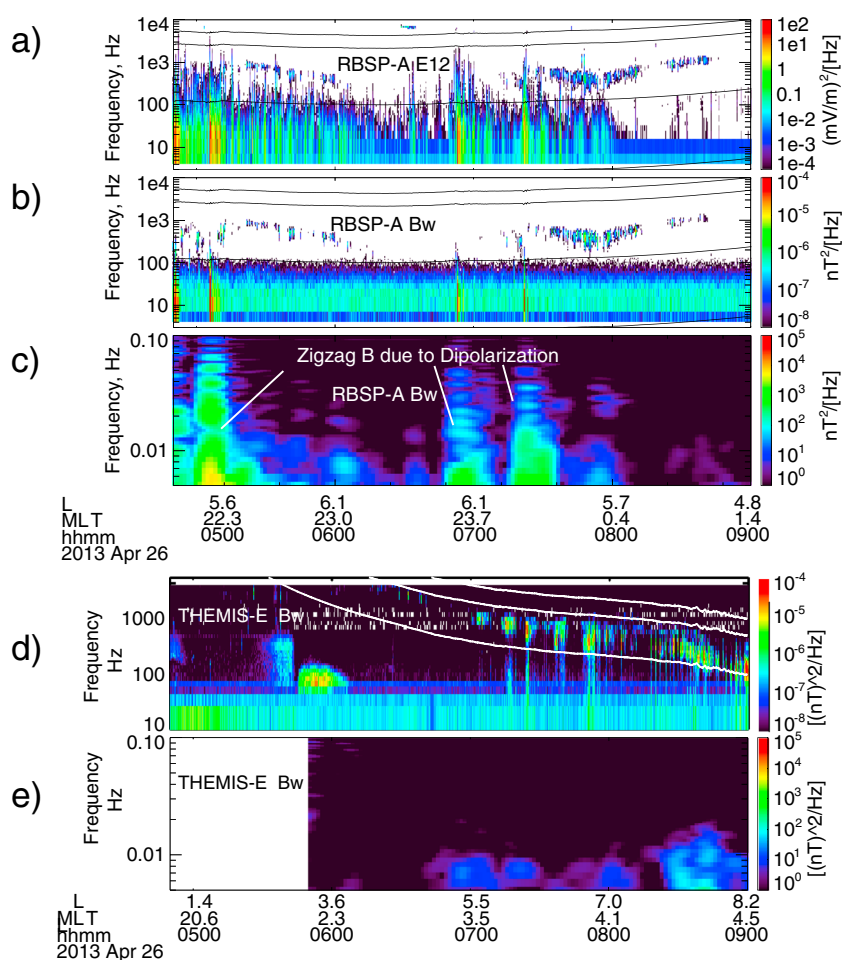


Figure 4. The observations of wave power spectra from RBSP-A and THEMIS-E. (a and b) RBSP-A observations of the wave power spectra (10^{-10^4} Hz) of one electric field component (**E12**) and one magnetic field component (**Bw**) from EFW burst data in VLF frequency range. (top to bottom) The three horizontal black lines in each panel represent the local electron gyrofrequency (f_{ce}), half f_{ce} , and the lower hybrid frequency. (c) RBSP-A observations of the power spectra in the ULF frequency band. (d and e) THEMIS-E observations of wave power spectra in the VLF frequency and ULF frequency band. The black region in Figure 4e is the inner radiation belt with strong DC magnetic fields.

Based on the above estimates, whistler wave-driven acceleration and radial diffusion are unlikely responsible for the MeV electron enhancement in Figure 3. We conclude that substorm injection is primarily responsible for increases of MeV electrons at $L > 4.8$ in this event. The PSD increase reflects a high PSD of source populations that were directly transported to RBSP. The inferred source of high PSD may relate to a positive gradient of PSD in radial direction [e.g., Turner *et al.*, 2010] or a transient process.

2.6. Schematic: The Dipolarization and Injection of MeV Electrons

The main dipolarization and injection observations are summarized in the schematic in Figure 5. Located at the nightside geosynchronous altitude, GOES 13 and LANL 94 first encountered the injection region at around 0502 UT. The dipolarization at GOES 13 was a large-scale dipolarization in which **Bz** and energetic electron fluxes increase to an elevated level. At 0506 UT, RBSP-A observed a small-scale dipolarization front. From the timing difference (3–4 min) of the dispersionless injection at GOES 13 and RBSP-A, the injection region propagated earthward at 30–40 km/s, consistent with previous statistic studies [Moore *et al.*, 1981; Reeves *et al.*, 1996]. The different characteristics of dipolarizations at these two spacecraft reflect a strong inhomogeneity of the injection region across the azimuthal direction and/or the radial direction. The observation of this event suggests a patchy, rapidly varying injection region.

As the injection region propagated earthward inside the geosynchronous altitude, the dipolarization electric field presumably was reduced at $L = 6.8$. Gradient **B** drift gradually became dominant, and particles started

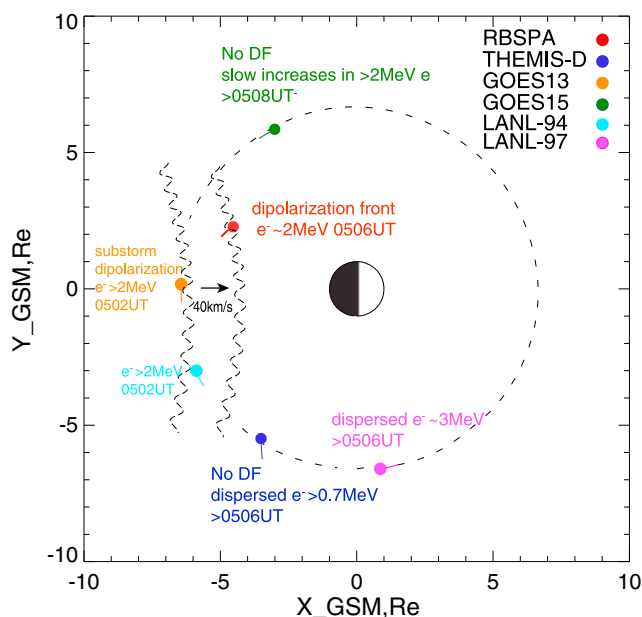


Figure 5. The xy plane schematic of RBSP-A, LANL-94, LANL-97, THEMIS-D, GOES 13, and GOES 15 during the dipolarization and injection of MeV electrons.

to drift away from the injection region. By 0506 UT when the injection region reached RBSP, large amounts of energetic electrons were released from the injection region. Outside the injection region, LANL 97 observed dispersed and drifting MeV electrons; THEMIS observed the energy-dispersive drifting electrons >700 keV, and GOES 15 observed slow MeV electrons increases. Based on the PSD results in Figure 3, the injection region may penetrate to $L = 4.8$.

3. Summary and Discussion

We present observations of an MeV electron injection event measured by RBSP at $L = 5.5$ and THEMIS, LANL-GEO, and GOES at geosynchronous altitude. This MeV electron injection event is particularly interesting because it featured a large (50 mV/m) duskward electric field pulse associated with a

dipolarization front at RBSP-A. Pitch angle observations indicated that betatron acceleration of the MeV electrons was operating at the dipolarization front. Dispersed, drifting MeV electrons were observed at LANL-GEO. Corresponding signals of MeV electron injection were also observed by GOES and THEMIS at the geosynchronous altitude. The injection region propagated earthward at a speed of 30–40 km/s inside the geosynchronous altitude. After a series of injections, the PSD of MeV electrons increased by an order of magnitude at $L > 4.8$ in less than 3 h. We show evidence that whistler wave-driven acceleration and radial diffusion are unlikely responsible for the MeV electron enhancement in this event. Our observations indicate that the deep injection associated with strong dipolarization electric fields can supply significant MeV electrons to the outer radiation belt.

Substorm injection can be thought of as a coherent radial transport process. The electric field must be intense and nonrandom during its interaction with particles for such coherent radial transport to be effective. A one to tens of MeV electron injection caused by shock-induced electric fields is an example of coherent transport [Blake et al., 1992; Li et al., 1993; Wygant et al., 1994]. The intensity and structure of dipolarization electric fields may be important in differentiating injections of MeV electrons from injections of subrelativistic electrons. The large magnitude of the dipolarization electric field (~ 50 mV/m) in this event far exceeded the values (several mV/m) used in most injection models. Regarding the electric field structure, our observations suggested that the injection region (and probably the dipolarization electric field) is likely to be patchy and/or rapidly-varying. These observations may shed lights on future efforts to model injections of MeV electrons.

Another important factor in MeV electron injections is the source population. During near-Earth injections, energetic electrons are transported earthward and trapped in the inner magnetosphere. The increase of PSD in Figure 3 reflects a high PSD of the source populations that were directly transported to the outer radiation belt. The high PSD of the source population needed for MeV electron injection may be from the high-energy tail of the plasma sheet populations, a temporal source in the magnetotail (e.g., reconnection), or accumulated from previous substorms.

References

Angelopoulos, V., W. Baumjohann, C. F. Kennel, F. V. Coroniti, M. G. Kivelson, R. Pellat, R. J. Walker, H. Luehr, and G. Paschmann (1992), Bursty bulk flows in the inner central plasma sheet, *J. Geophys. Res.*, *97*, 4027–4039, doi:10.1029/91JA02701.

Ashour-Abdalla, M., M. El-Alaoui, M. L. Goldstein, M. Zhou, D. Schriver, R. Richard, R. Walker, M. G. Kivelson, and K.-J. Hwang (2011), Observations and simulations of non-local acceleration of electrons in magnetotail magnetic reconnection events, *Nat. Phys.*, *7*, 360–365, doi:10.1038/nphys1903.

Acknowledgments

This work was supported by NNSFC grant 41231067 and in part by the Specialized Research Fund for State Key Laboratories of China. Work at UMN was supported by a contract from APL for the development of RBSP/EFW. EMFISIS is supported by a JHU/APL contract 921647. L.C. would like to acknowledge the support of the NASA grant NNX15AF55G. D.L.T., G.D.R., and X.L. are thankful for the support from the International Space Science Institute's (ISSI) International Teams program. L.D. greatly appreciates Judy Hohl from UCLA for editorial help. The RBSP EMFISIS data are available at <http://emfisis.physics.uiowa.edu/Flight/>. The RBSP EFW data are available at <http://rbsp.space.umn.edu/data/rbsp/>. The RBSP ECT data are available at <http://www.rbsp-ect.lanl.gov/>. THEMIS data are available at <http://themis.ssl.berkeley.edu/data/themis/>. LANL-GEO data are provided by Geoffrey D. Reeves. GOES data are available at <http://satdat.ngdc.noaa.gov/sem/goes/data/>. The OMNI data are available at CDAWeb. The SYM-H data are provided by the World Data Center for Geomagnetism, Kyoto.

The Editor thanks two anonymous reviewers for their assistance in evaluating this paper.

- Baker, D. N., T. I. Pulkkinen, V. Angelopoulos, W. Baumjohann, and R. L. McPherron (1996), Neutral line model of substorms: Past results and present view, *J. Geophys. Res.*, *101*, 12,975–13,010, doi:10.1029/95JA03753.
- Baker, D. N., et al. (2013), The Relativistic Electron-Proton Telescope (REPT) instrument on board the Radiation Belt Storm Probes (RBSP) spacecraft: Characterization of Earth's radiation belt high-energy particle populations, *Space Sci. Rev.*, *179*, 337–381, doi:10.1007/s11214-012-9950-9.
- Birn, J., M. F. Thomsen, J. E. Borovsky, G. D. Reeves, D. J. McComas, R. D. Belian, and M. Hesse (1998), Substorm electron injections: Geosynchronous observations and test particle simulations, *J. Geophys. Res.*, *103*, 9235–9248, doi:10.1029/97JA02635.
- Birn, J., M. Hesse, R. Nakamura, and S. Zaharia (2013), Particle acceleration in dipolarization events, *J. Geophys. Res. Space Physics*, *118*, 1960–1971, doi:10.1002/jgra.50132.
- Blake, J., et al. (2013), The Magnetic Electron Ion Spectrometer (MagEIS) instruments aboard the Radiation Belt Storm Probes (RBSP) spacecraft, *Space Sci. Rev.*, 1–39, doi:10.1007/s11214-013-9991-8.
- Blake, J. B., W. A. Kolasinski, R. W. Fillius, and E. G. Mullen (1992), Injection of electrons and protons with energies of tens of MeV into L less than 3 on 24 March 1991, *Geophys. Res. Lett.*, *19*, 821–824, doi:10.1029/92GL00624.
- Cattell, C. A., and F. S. Mozer (1984), Substorm electric fields in the Earth's magnetotail, in *Magnetic Reconnection in Space and Laboratory Plasmas*, pp. 208–215, AGU, Washington, D. C.
- Chen, Y., R. H. W. Friedel, G. D. Reeves, T. G. Onsager, and M. F. Thomsen (2005), Multisatellite determination of the relativistic electron phase space density at geosynchronous orbit: Methodology and results during geomagnetically quiet times, *J. Geophys. Res.*, *110*, A10210, doi:10.1029/2004JA010895.
- Dai, L., et al. (2013), Excitation of poloidal standing Alfvén waves through drift resonance wave-particle interaction, *Geophys. Res. Lett.*, *40*, 4127–4132, doi:10.1002/grl.50800.
- Dai, L., J. R. Wygant, C. A. Cattell, S. Thaller, K. Kersten, A. Breneman, X. Tang, R. H. Friedel, S. G. Claudepierre, and X. Tao (2014), Evidence for injection of relativistic electrons into the Earth's outer radiation belt via intense substorm electric fields, *Geophys. Res. Lett.*, *41*, 1133–1141, doi:10.1002/2014GL059228.
- Fairfield, D. H., et al. (1998), Geotail observations of substorm onset in the inner magnetotail, *J. Geophys. Res.*, *103*, 103–118, doi:10.1029/97JA02043.
- Fok, M.-C., T. E. Moore, and W. N. Spjeldvik (2001), Rapid enhancement of radiation belt electron fluxes due to substorm dipolarization of the geomagnetic field, *J. Geophys. Res.*, *106*, 3873–3882, doi:10.1029/2000JA000150.
- Fok, M.-C., T. E. Moore, P. C. Brandt, D. C. Delcourt, S. P. Slinker, and J. A. Fedder (2006), Impulsive enhancements of oxygen ions during substorms, *J. Geophys. Res.*, *111*, A10222, doi:10.1029/2006JA011839.
- Friedel, R. H. W., A. Korth, and G. Kremser (1996), Substorm onsets observed by CRRES: Determination of energetic particle source regions, *J. Geophys. Res.*, *101*, 13,137–13,154, doi:10.1029/96JA00399.
- Fu, H. S., Y. V. Khotyaintsev, M. André, and A. Vaivads (2011), Fermi and betatron acceleration of suprathermal electrons behind dipolarization fronts, *Geophys. Res. Lett.*, *38*, L16104, doi:10.1029/2011GL048528.
- Gabrielse, C., V. Angelopoulos, A. Runov, and D. L. Turner (2012), The effects of transient, localized electric fields on equatorial electron acceleration and transport toward the inner magnetosphere, *J. Geophys. Res.*, *117*, A10213, doi:10.1029/2012JA017873.
- Ge, Y. S., J. Raeder, V. Angelopoulos, M. L. Gilson, and A. Runov (2011), Interaction of dipolarization fronts within multiple bursty bulk flows in global MHD simulations of a substorm on 27 February 2009, *J. Geophys. Res.*, *116*, A00123, doi:10.1029/2010JA015758.
- Glocer, A., M.-C. Fok, T. Nagai, G. Tóth, T. Guild, and J. Blake (2011), Rapid rebuilding of the outer radiation belt, *J. Geophys. Res.*, *116*, A09213, doi:10.1029/2011JA016516.
- Horne, R. B., R. M. Thorne, S. A. Glauert, J. M. Albert, N. P. Meredith, and R. R. Anderson (2005), Timescale for radiation belt electron acceleration by whistler mode chorus waves, *J. Geophys. Res.*, *110*, A03225, doi:10.1029/2004JA010811.
- Hwang, K.-J., M. L. Goldstein, E. Lee, and J. S. Pickett (2011), Cluster observations of multiple dipolarization fronts, *J. Geophys. Res.*, *116*, A00132, doi:10.1029/2010JA015742.
- Ingraham, J. C., T. E. Cayton, R. D. Belian, R. A. Christensen, R. H. W. Friedel, M. M. Meier, G. D. Reeves, and M. Tuszewski (2001), Substorm injection of relativistic electrons to geosynchronous orbit during the great magnetic storm of March 24, 1991, *J. Geophys. Res.*, *106*, 25,759–25,776, doi:10.1029/2000JA000458.
- Kim, H.-J., A. A. Chan, R. A. Wolf, and J. Birn (2000), Can substorms produce relativistic outer belt electrons?, *J. Geophys. Res.*, *105*, 7721–7736, doi:10.1029/1999JA900465.
- Kletzing, C., et al. (2013), The Electric and Magnetic Field Instrument Suite and Integrated Science (EMFISIS) on RBSP, *Space Sci. Rev.*, *179*, 127–181, doi:10.1007/s11214-013-9993-6.
- Li, W., R. M. Thorne, V. Angelopoulos, J. Bortnik, C. M. Cully, B. Ni, O. LeContel, A. Roux, U. Auster, and W. Magnes (2009), Global distribution of whistler-mode chorus waves observed on the THEMIS spacecraft, *Geophys. Res. Lett.*, *36*, L09104, doi:10.1029/2009GL037595.
- Li, X., I. Roth, M. Temerin, J. R. Wygant, M. K. Hudson, and J. B. Blake (1993), Simulation of the prompt energization and transport of radiation belt particles during the March 24, 1991 SSC, *Geophys. Res. Lett.*, *20*, 2423–2426, doi:10.1029/93GL02701.
- Li, X., D. N. Baker, M. Temerin, G. D. Reeves, and R. D. Belian (1998), Simulation of dispersionless injections and drift echoes of energetic electrons associated with substorms, *Geophys. Res. Lett.*, *25*, 3763–3766, doi:10.1029/1998GL900001.
- Li, X., T. E. Sarris, D. N. Baker, W. K. Peterson, and H. J. Singer (2003), Simulation of energetic particle injections associated with a substorm on August 27, 2001, *Geophys. Res. Lett.*, *30*(1), 1004, doi:10.1029/2002GL015967.
- Liu, J., V. Angelopoulos, A. Runov, and X.-Z. Zhou (2013), On the current sheets surrounding dipolarizing flux bundles in the magnetotail: The case for wedgelets, *J. Geophys. Res. Space Physics*, *118*, 2000–2020, doi:10.1002/jgra.50092.
- Liu, W. L., X. Li, T. Sarris, C. Cully, R. Ergun, V. Angelopoulos, D. Larson, A. Keiling, K. H. Glassmeier, and H. U. Auster (2009), Observation and modeling of the injection observed by THEMIS and LANL satellites during the 23 March 2007 substorm event, *J. Geophys. Res.*, *114*, A00C18, doi:10.1029/2008JA013498.
- Mauk, B. H., N. J. Fox, S. G. Kanekal, R. L. Kessel, D. G. Sibeck, and A. Ukhorskiy (2012), Science objectives and rationale for the Radiation Belt Storm Probes mission, *Space Sci. Rev.*, *179*, 3–27, doi:10.1007/s11214-012-9908-y.
- Moore, T. E., R. L. Arnoldy, J. Feynman, and D. A. Hardy (1981), Propagating substorm injection fronts, *J. Geophys. Res.*, *86*, 6713–6726, doi:10.1029/JA086iA08p06713.
- Nagai, T., A. S. Yukimatu, A. Matsuoka, K. T. Asai, J. C. Green, T. G. Onsager, and H. J. Singer (2006), Timescales of relativistic electron enhancements in the slot region, *J. Geophys. Res.*, *111*, A11205, doi:10.1029/2006JA011837.
- Nakamura, R., et al. (2002), Motion of the dipolarization front during a flow burst event observed by Cluster, *Geophys. Res. Lett.*, *29*(20), 1942, doi:10.1029/2002GL015763.
- Nakamura, R., et al. (2011), Flux transport, dipolarization, and current sheet evolution during a double-onset substorm, *J. Geophys. Res.*, *116*, A00136, doi:10.1029/2010JA015865.

- Northrop, T. G. (1963), Adiabatic charged-particle motion, *Rev. Geophys. Space Phys.*, *1*, 283–304.
- Ozeke, L. G., I. R. Mann, K. R. Murphy, I. J. Rae, D. K. Milling, S. R. Elkington, A. A. Chan, and H. J. Singer (2012), ULF wave derived radiation belt radial diffusion coefficients, *J. Geophys. Res.*, *117*, A04222, doi:10.1029/2011JA017463.
- Reeves, G. D., R. D. Belian, and T. A. Fritz (1991), Numerical tracing of energetic particle drifts in a model magnetosphere, *J. Geophys. Res.*, *96*, 13,997–14,008, doi:10.1029/91JA01161.
- Reeves, G. D., M. G. Henderson, P. S. McLachlan, R. D. Belian, R. H. W. Friedel, and A. Korth (1996), Radial propagation of substorm injections, in *International Conference on Substorms*, vol. 389, edited by E. J. Rolfe and B. Kaldeich, pp. 579–584, ESA Spec. Publ., Paris.
- Rowland, D. (2002), The electrodynamics of the inner magnetosphere during major geomagnetic storms, PhD thesis, Univ. Of Minnesota, Minnesota.
- Runov, A., V. Angelopoulos, M. I. Sitnov, V. A. Sergeev, J. Bonnell, J. P. McFadden, D. Larson, K.-H. Glassmeier, and U. Auster (2009), THEMIS observations of an earthward-propagating dipolarization front, *Geophys. Res. Lett.*, *36*, L14106, doi:10.1029/2009GL038980.
- Sarris, T. E., X. Li, N. Tsaggas, and N. Paschalidis (2002), Modeling energetic particle injections in dynamic pulse fields with varying propagation speeds, *J. Geophys. Res.*, *107*(A3), 1033, doi:10.1029/2001JA900166.
- Sergeev, V. A., M. A. Shukhtina, R. Rasinkangas, A. Korth, G. D. Reeves, H. J. Singer, M. F. Thomsen, and L. I. Vagina (1998), Event study of deep energetic particle injections during substorm, *J. Geophys. Res.*, *103*, 9217–9234, doi:10.1029/97JA03686.
- Spence, H. E., et al. (2013), Science goals and overview of the Radiation Belt Storm Probes (RBSP) Energetic Particle, Composition, and Thermal Plasma (ECT) suite on NASA's Van Allen Probes mission, *Space Sci. Rev.*, *179*, 311–336, doi:10.1007/s11214-013-0007-5.
- Su, Z., et al. (2014), Quantifying the relative contributions of substorm injections and chorus waves to the rapid outward extension of electron radiation belt, *J. Geophys. Res. Space Physics*, *119*, 10,023–10,040, doi:10.1002/2014JA020709.
- Tsyganenko, N. A., and M. I. Sitnov (2005), Modeling the dynamics of the inner magnetosphere during strong geomagnetic storms, *J. Geophys. Res.*, *110*, A03208, doi:10.1029/2004JA010798.
- Tu, J.-N., K. Tsuruda, H. Hayakawa, A. Matsuoka, T. Mukai, I. Nagano, and S. Yagitani (2000), Statistical nature of impulsive electric fields associated with fast ion flow in the near-Earth plasma sheet, *J. Geophys. Res.*, *105*, 18,901–18,908, doi:10.1029/1999JA000428.
- Turner, D., et al. (2015), Energetic electron injections deep into the inner magnetosphere associated with substorm activity, *Geophys. Res. Lett.*, *42*, 2079–2087, doi:10.1002/2015GL063225.
- Turner, D. L., X. Li, G. D. Reeves, and H. J. Singer (2010), On phase space density radial gradients of Earth's outer-belt electrons prior to sudden solar wind pressure enhancements: Results from distinctive events and a superposed epoch analysis, *J. Geophys. Res.*, *115*, A01205, doi:10.1029/2009JA014423.
- Wygant, J., F. Mozer, M. Temerin, J. Blake, N. Maynard, H. Singer, and M. Smiddy (1994), Large amplitude electric and magnetic field signatures in the inner magnetosphere during injection of 15 MeV electron drift echoes, *Geophys. Res. Lett.*, *21*, 1739–1742, doi:10.1029/94GL00375.
- Wygant, J. R., et al. (2013), The electric field and waves instruments on the Radiation Belt Storm Probes mission, *Space Sci. Rev.*, *179*, 183–220, doi:10.1007/s11214-013-0013-7.
- Yang, J., F. R. Toffoletto, R. A. Wolf, and S. Sazykin (2011), RCM-E simulation of ion acceleration during an idealized plasma sheet bubble injection, *J. Geophys. Res.*, *116*, A05207, doi:10.1029/2010JA016346.
- Zaharia, S., J. Birn, R. H. W. Friedel, G. D. Reeves, M. F. Thomsen, and C. Z. Cheng (2004), Substorm injection modeling with nondipolar, time-dependent background field, *J. Geophys. Res.*, *109*, A10211, doi:10.1029/2004JA010464.
- Zhang, J.-C., R. A. Wolf, R. W. Spiro, G. M. Erickson, S. Sazykin, F. R. Toffoletto, and J. Yang (2009), Rice convection model simulation of the substorm-associated injection of an observed plasma bubble into the inner magnetosphere: 2. Simulation results, *J. Geophys. Res.*, *114*, A08219, doi:10.1029/2009JA014131.
- Zhou, X.-Z., V. Angelopoulos, J. Liu, A. Runov, and S.-S. Li (2014), On the origin of pressure and magnetic perturbations ahead of dipolarization fronts, *J. Geophys. Res. Space Physics*, *119*, 211–220, doi:10.1002/2013JA019394.